We are IntechOpen, the world's leading publisher of Open Access books Built by scientists, for scientists

4,800
Open access books available

122,000
International authors and editors

135M
Downloads

Our authors are among the

154
Countries delivered to

TOP 1%
most cited scientists

12.2%
Contributors from top 500 universities

CLARIVATE ANALYTICS BOOK CITATION INDEX INDEXED

WEB OF SCIENCE™

Selection of our books indexed in the Book Citation Index in Web of Science™ Core Collection (BKCI)

Interested in publishing with us?
Contact book.department@intechopen.com

Numbers displayed above are based on latest data collected.
For more information visit www.intechopen.com

14

Simulations of Unusual Properties of Water Inside Carbon Nanotubes

Yoshimichi Nakamura and Takahisa Ohno
National Institute for Materials Science; CREST-JST
Japan

1. Introduction

Water, which is vital for all living creatures and essential to our daily lives, is one of the most researched materials on earth. It is amazing to see that even after a long history of research, this substance consisting of triatomic molecules is still rich in new discoveries on its unexpected properties. Among the hottest topics over the last decade is anomalous behavior of water molecules inside confined nanospaces, which stimulates our scientific curiosity from the viewpoint of how the tiny, polar molecules rearrange themselves when strongly confined. What the hydrogen-bond network is like? In this research field, molecular dynamics (MD) simulations have played a leading role and are expected to further increase its importance in predicting unexpected properties of water. Typical of well-defined, size-controlled nanospaces easily obtainable is the interior space of carbon nanotubes (CNTs). Figure 1 shows the relation of a single-walled CNT to the graphene honeycomb lattice. An example where the graphene lattice vector $m\mathbf{a1} + m\mathbf{a2}$ corresponds to the circumference of the CNT is shown in the figure. This type of CNT is typically referred to in this chapter and the pair of integers (m, m) is often quoted as a useful index of the CNT diameter.

When exploring a new ordered phase of the water molecules, it is quite natural and reasonable to focus on low-temperature/high-pressure conditions. MD simulation is a powerful tool for such exploration. In the CNT diameter range about 1-2 nm, the water molecules were reported to be frozen into a variety of forms of 'ice nanotube' inside the CNT (Bai et al., 2006; Koga at al., 2001; Luo et al., 2008; Mikami et al., 2009). For example, at P = 500 bar and T ≤ 240 K, 4-, 5-, and 6-gonal ice nanotubes were observed for (14, 14), (15, 15) and (16, 16) CNTs, respectively (Koga et al., 2001). All those simulations on ice-nanotubes were performed with the use of infinite or capped CNTs, which means that the confined water density can be directly controlled. In one of such MD simulation studies, a double-layered helix form was demonstrated to be possible inside the infinite (10, 10) CNT at 298K for the confined water density of '1 g/cc' (Liu et al., 2005). Here, the water density was estimated based on the number of confined molecules divided by the geometrical volume of the CNT, not by its effective inner space volume, which is at most about 60% of the geometrical volume for the (10, 10) CNT due to the hydrophobic nature of the CNT wall. The value of '1 g/cc' therefore corresponds to a very high density condition.

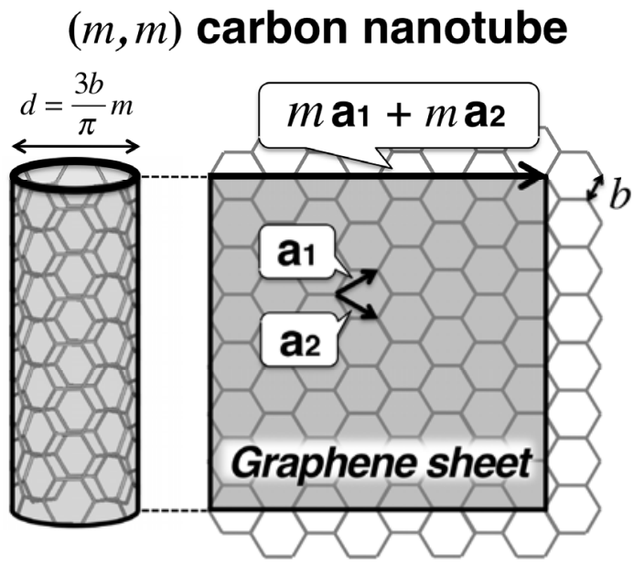

Fig. 1. Illustration of an (*m, m*) carbon nanotube and a graphene sheet.

Amazingly, at ambient conditions (300K, 1 bar) another ordered phase similar to the 6-gonal ice nanotube was found inside uncapped (9, 9) CNTs (Mashl. et al., 2003). The new phase reveals ice-like mobility with an amount of hydrogen bonding similar to that in the bulk liquid water. Unlike the simulations using infinite or capped CNTs, each water molecule was allowed to enter (leave) the CNTs from (for) the outside bulk water. The interior of the uncapped CNTs is therefore naturally filled with water molecules. The uncapped CNTs were embedded into wafers of neutral atoms mimicking the hydrophobic interior of a phospholipid membrane. Based on the same water model used in the above study, i.e., the SPC/E model (Berendsen et al., 1987), we have confirmed that the anomalously immobilized water at ambient conditions is also observed inside the uncapped CNTs which is NOT embedded into the membrane but directly immersed in a water reservoir (Fig. 2).

It should be noted that a more recent MD study has reported a brand new water phase called 'ferroelectric mobile water (FMW)' (Nakamura & Ohno, 2011, 2012a, 2012b). Though the FMW at first sight appears similar to the immobilized water mentioned above, they are distinct from each other both in molecular structure and in dynamics. The FMW is produced inside (8, 8) and (9, 9) CNTs immersed in a water reservoir at ambient conditions based on the TIP5P-E model (Rick, 2004). The details of the FMW will be explained later.

The H_2O/CNT simulation studies have thus revealed a variety of unusual properties of water molecules and improved our general knowledge of water and ice. Also, knowledge on influential factors such as the CNT diameter, temperature, and pressure has been increasing. For spontaneous filling of CNTs with liquid water, there are many simulations employing a similar set of these conditions. We see, however, that in some cases they do not always yield the similar results. This implies that difference in water models used is potentially another important influential factor to be considered. In this chapter, therefore, paying attention to the effect of water models, we explore the unusual behaviour of the confined water.

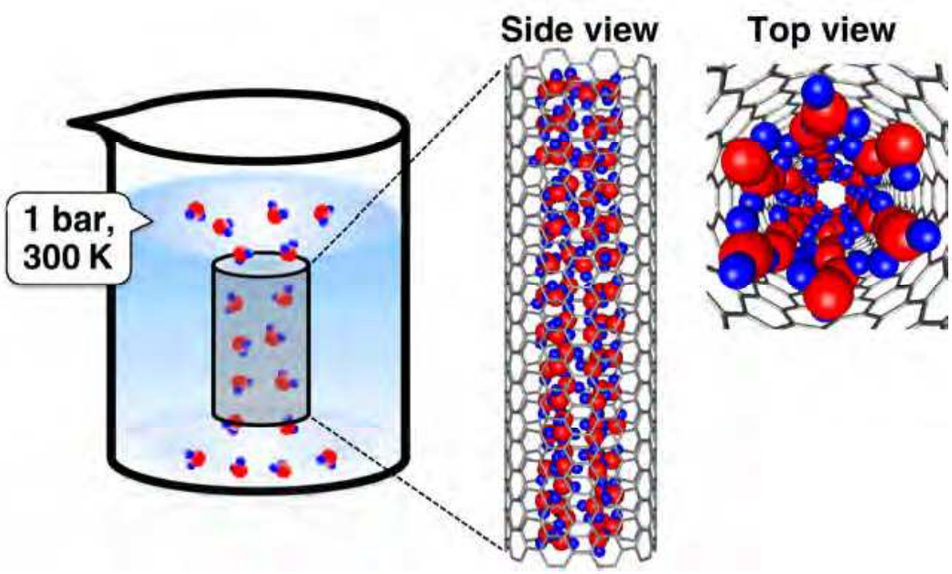

Fig. 2. Left: Illustration of an uncapped CNT in a water reservoir. Right: Snapshots of anomalously immobilized water at ambient conditions. Simulations are performed for the (9, 9) CNTs immersed in a water reservoir based on the SPC/E water model. Red for oxygen, blue for hydrogen.

2. Overview of water models

Figure 3 shows a series of the transferable interaction potentials for water molecules, TIP*n*P models (Jorgenen et al., 1983; Mohoney & Jorgensen, 2000), demonstrating how the water models are classified from the viewpoint of the number of interaction sites (denoted by *n*). The models for n = 3, 4, and 5 are represented in the figure. All models use the same rigid molecular structure. The van der Waals (vdW) interaction is commonly described by the 6-12 Lennard-Jones potential between the oxygen atom sites (closed black circles). Significant differences among the models are in the description of the electrostatic interaction sites (open white circles).

In the TIP3P model, the molecular charge distribution is modeled by point charges on each nuclei (Fig. 3, lower left). Together with the vdW site, the total number of interaction sites is three, as the model's name implies. In the TIP4P model, unlike in the TIP3P model, the negative charge is placed on an additional fictive site, resulting in four interaction sites overall (Fig. 3, lower middle). In the TIP5 model, the charge distribution is more realistically treated. The negative charges along the lone-pair directions are explicitly taken into account (Fig. 3, lower right).

At the expense of more computational cost than the 3- and 4-site models, the 5-site model have succeeded in reproducing more of the water properties over a range of temperatures and pressures, including the density maximum near 4 °C (Mohoney & Jorgensen, 2000) and the melting point (Fernández et al., 2006; Vega eat al., 2005). There has also been proposed a modified version of the TIP5P, called TIP5P-E (Rick, 2004), which is constructed by only modifying the Lennard-Jones parameters so as to yield more accurate results when used with Ewald sum calculations for long-ranged electrostatic interactions.

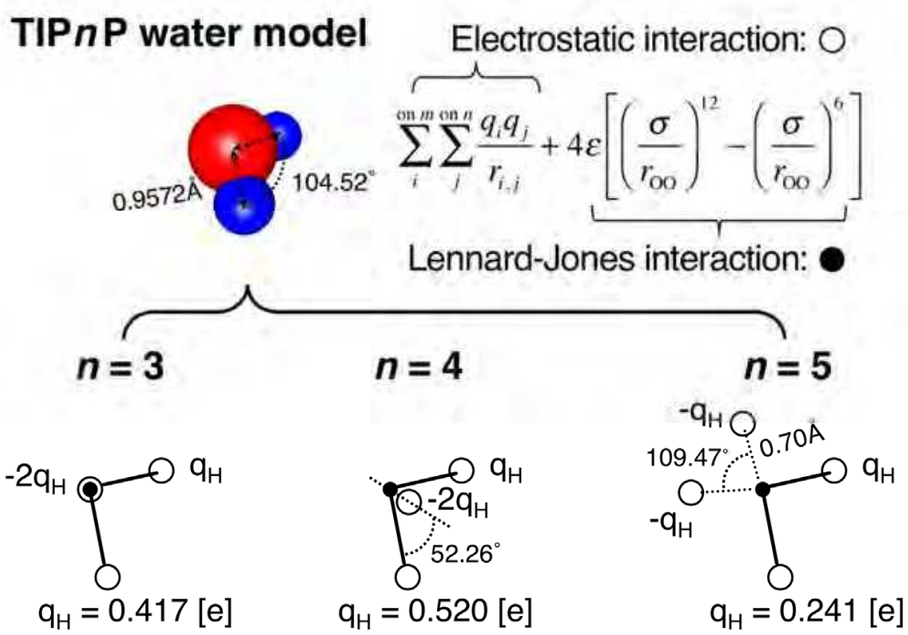

Fig. 3. Illustration of TIP*n*P water models. Red for oxygen, blue for hydrogen.

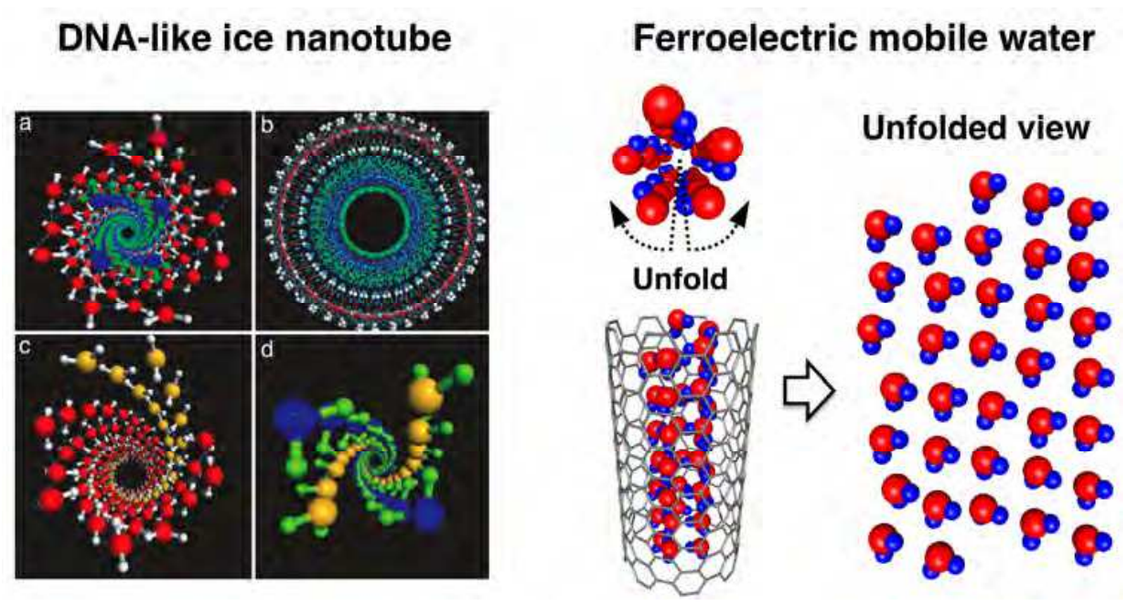

Fig. 4. Examples of H_2O/CNT simulation results based on 5-site water models (left figure is from Fig.1 of Bai et al., 2006. Copyright 2006 National Academy of Sciences.)

The TIP3P and TIP4P models have been the most commonly used water models, along with other variations of 3-site models, SPC and SPC/E (Berendsen et al., 1981, 1987). Such is also the case for H_2O/CNT simulations. Though the number of H_2O/CNT simulation studies based on the 5-site models is only a few, their findings that the water molecules are able to self-assemble into double helixes resembling DNA under high pressure (Bai at al., 2006) and that single-domain ferroelectric mobile water is possible at ambient conditions (Nakamura

& Ohno, 2011, 2012a, 2012b) are all the more outstanding, considering far more numerous studies based on the 3- and 4-site models.

3. Spontaneous filling of CNTs with liquid water

Regarding the spontaneous filling of CNTs with liquid water, various 3-site water models have been tried for a wide range of CNT diameter (Alexiadis & Kassinos, 2008a, 2008b). It was shown that the different choices of rigid/flexible model for the TIP3P, SPC, and SPC/E water molecules, along with rigid/flexible choices of CNTs, cause no significant differences. We now perform systematic simulations based on not only 3-site water models (TIP3P and SPC/E) but also 4-site (TIP4P) and 5-site (TIP5P-E) models (Nakamura & Ohno, 2012a).

A nonpolar, rigid (*m, m*) CNT of length *L* is solvated with *N* water molecules in a periodic box. *L* = 2.1 nm for *m* = 6, 7, 8, 9, 10, 12, 16, 20 (0.8 - 2.7 nm in diameter). *L* = 4.0 nm for *m* = 8, 9. *N* ranges from 2074 to 6508, depending on the CNT size. The carbon-carbon bond length is 1.4 Å. MD simulations are performed using AMBER 9.0 (Case et al., 2006). The water molecules and the CNTs are assumed to interact through the 6-12 Lennard-Jones potential between the oxygen and the sp^2 carbon atoms (AMBER force field). Based on the cross section σ_{OO} (Table 1) and σ_{CC} (3.4 Å), and the depth of the potential well ε_{OO} (Table 1) and ε_{CC} (0.086 kcal/mol), σ_{CO} and ε_{CO} are derived from the Lorentz-Berthelot combining rules,

$$\varepsilon_{CO} = \sqrt{\varepsilon_{CC} \times \varepsilon_{OO}}, \quad \sigma_{CO} = \frac{\sigma_{CC} + \sigma_{OO}}{2} . \tag{1}$$

Electrostatic interactions between the water molecules are calculated by particle-mesh Ewald method (Darden, 1993). An MD time step of 2 fsec is used. In the first runs (up to 0.5-0.6 nsec), a combination of constant volume and constant pressure simulations is performed to ensure the system is in equilibrium with the bulk water density at *T* K under 1 bar. In the subsequent MD time steps (10-120 nsec), the NVT-ensemble is used for statistical analysis. Snapshots are saved for analysis every 0.1 psec.

	TIP3P	SPC/E	TIP4P	TIP5P-E
σ_{OO} [Å]	3.15061	3.166	3.15365	3.097
ε_{OO} [kcal/mol]	0.1521	0.1553	0.1550	0.178

Table 1. Lennard-Jones potential parameters for each model.

Figure 5 shows the water density inside the CNTs, together with snapshots obtained by using the TIP5P-E model. As was already reported by the simulations based on the 3-site models, those based on the 4- and 5-site models also have three different filling modes, that is, 'wire', 'layered', and 'bulk' mode as the diameter size increases (Alexiadis & Kassinos, 2008a, 2008b).

In the wire mode, the water molecules form into a water wire regardless of the water model. Figure 5a shows a snapshot example of the single-file formation of the TIP5P-E molecules inside the (6, 6) CNT. It has been reported that the TIP3P water molecules in the wire mode undergo a burst-like transmission through the CNT (Hummer et al., 2001). A similar

concerted and rapid axial motion is observed also for the other water models. An example for the TIP5P-E model is shown in Fig. 6. In the wire mode, significant differences among the water models are not seen in both the structure and dynamics of the confined water molecules.

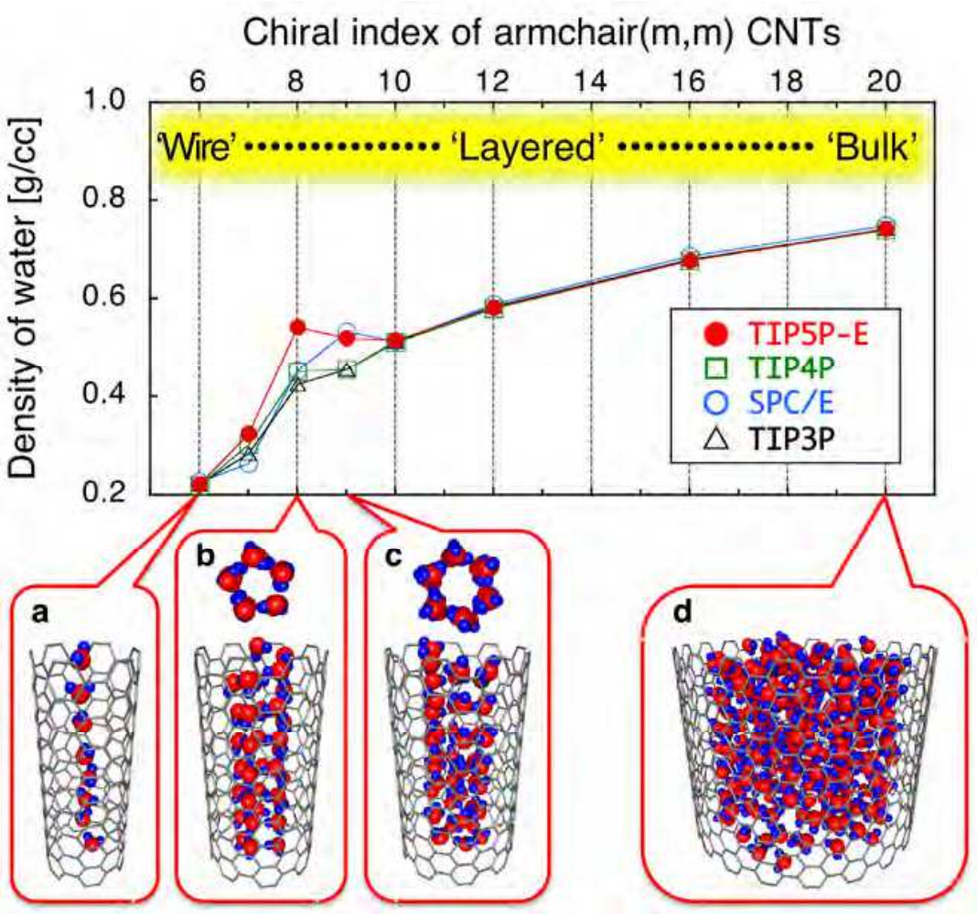

Fig. 5. Upper: Water density inside (*m, m*) CNTs of length 2.1 nm at 280 K. Data are from Fig.1b of Nakamura & Ohno, 2012a. Lower: Snapshots from MD simulations based on TIP5P-E model. (a) Single-file formation in 'wire' mode. (b) (c) Single-layered formation in 'layered' mode. (d) Example in 'Bulk' mode.

In the 'layered' mode, the larger the CNT diameter size, the more concentric layers of the confined water molecules come to appear. At the same time, those water layers become more diffuse and the bulk water structure gradually recovers. A snapshot example practically corresponding to the 'bulk' mode is shown in Fig. 5d.

The overall trend of the confined water density is that the shorter the diameter, the smaller the density. The density values for each model are practically the same except for the (8, 8) and (9, 9) CNTs (about 1.1-1.2 nm in CNT diameter). We notice that the TIP5P-E water density does not follow the overall trend for the (8, 8) and the (9, 9) CNT. The SPC/E water density does not follow the trend for the (9, 9) CNT. Inside the (8, 8) and (9, 9) CNTs, the TIP5P-E water molecules form into a single-layered water tube as shown in Fig. 5b and c.

Though they at first sight resemble the 5-gonal and 6-gonal ice nanotubes (Koga et al., 2001; Luo et al., 2008; Mikami et al., 2009), they are quite distinct from those ice nanotubes as explained in the next section.

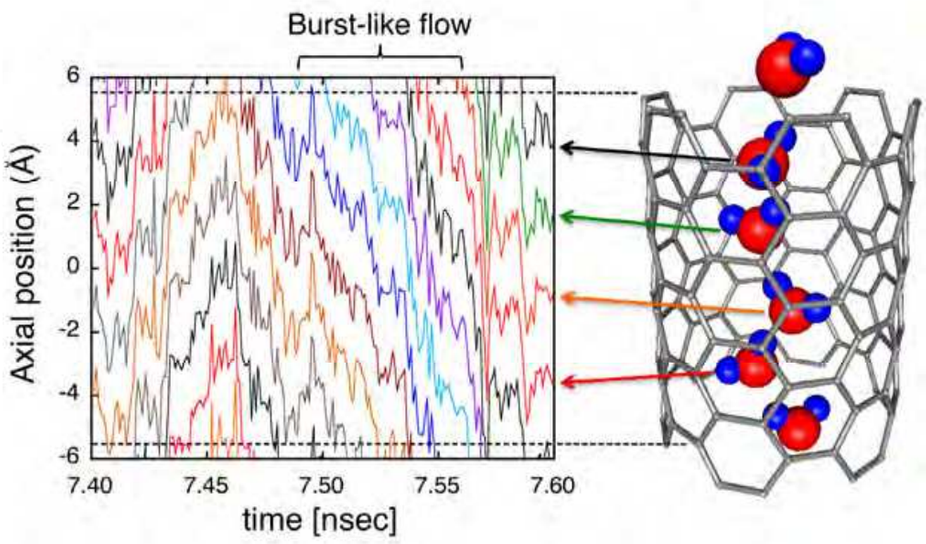

Fig. 6. Burst-like flow of the TIP5P-E water molecules along the CNT axis at 300 K.

4. Ferroelectric mobile water (FMW)

We look into the structure of the single-layered TIP5P-E water tubes inside the (8, 8) and (9, 9) CNTs. They are practically one-atom-thick water tubes as we see their top views in Fig. 5b and c. To detail the molecular structure, we unfold the water tube as shown in the upper part of Fig. 7. All the water molecules are visited by following one single helix running through the CNT. To our surprise, the dipole moment of each molecule is oriented in practically the same direction, which results in a single-domain ferroelectric arrangement of the water molecules and consequently a large spontaneous polarization along the CNT axis (Fig. 7, right-hand side). This new water phase is termed 'ferroelectric mobile water (FMW).' Its 'mobile' character will be explained later.

In Fig. 7, the direction of the axial spontaneous polarization is downward for the (8, 8) CNT and upward for the (9, 9) CNT. Each direction is observed as unchanged at least over about 100 ns. Of course, there is no reason for the net axial polarization to prefer one direction over the other. For reference, we tried other series of simulations using a different random arrangement of the water molecules, and obtained the opposite polarization direction for each. We also find that the longer the CNT length, the more stable the polarization direction. That is, employing the longer CNTs has an effect similar to reducing the temperature.

The unfolded-view snapshots in Fig. 7 reveal that a hydrogen bond network is completed, i.e., the 'ice rule' is obeyed (Bernal & Fowler, 1933). Moreover, the protons are perfectly ordered (Fig. 7, unfolded views in middle). Here, it is worth referring to proton-ordered ice (Pauling, 1935; Slater, 1941; Jackson & Whitworth, 1995; Jackson et al., 1997; Su et al., 1998; Iedema et al., 1998; Bramwell, 1999;). In ordinary ice (i.e., ice Ih), the protons are disordered though the ice rule is obeyed for its hexagonal lattice of the water molecules. The proton

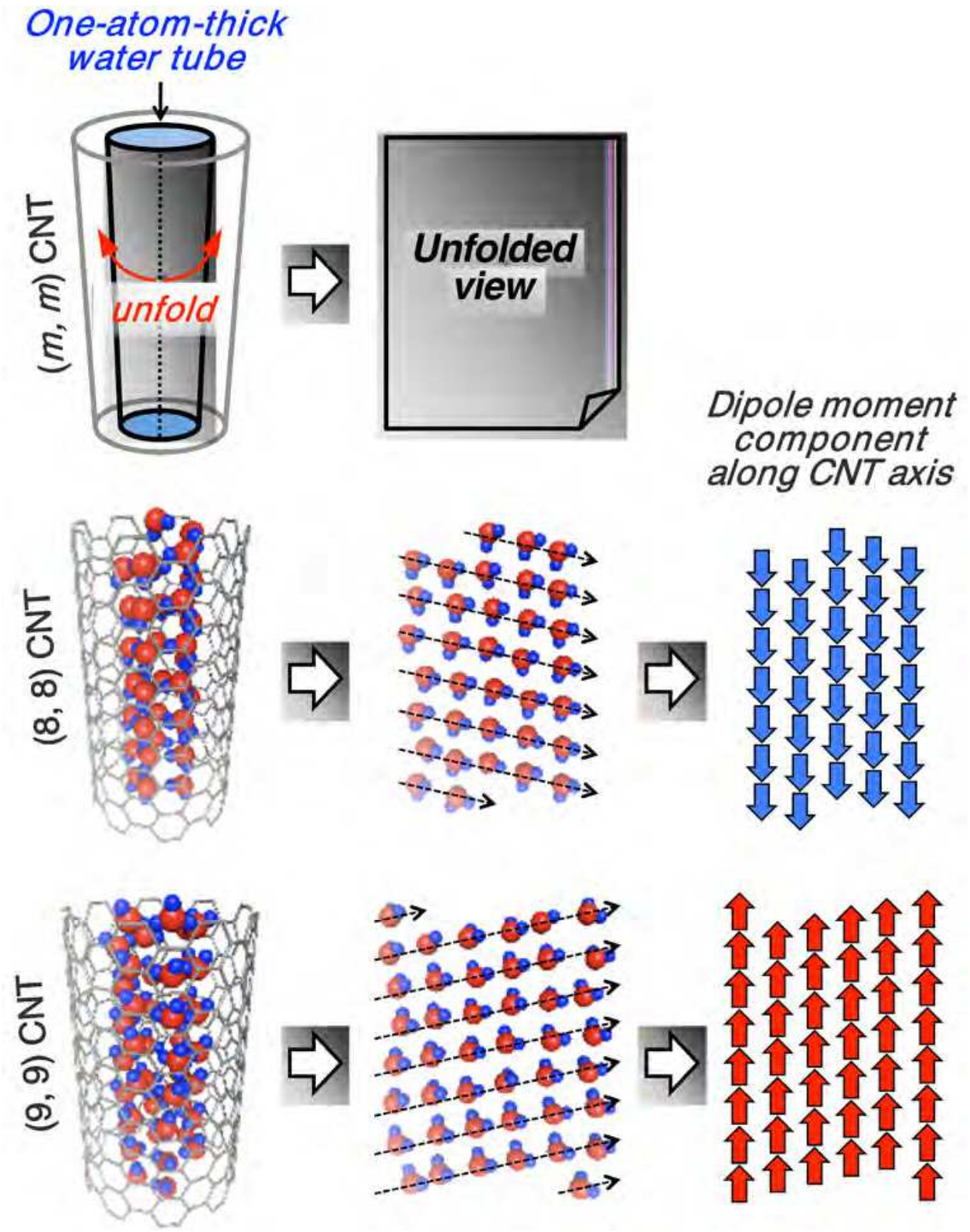

Fig. 7. Left: Side views of single-layered, one-atom-thick water tubes inside CNTs. Middle: Unfolded-views of TIP5P-E water molecules inside the (8, 8) and the (9, 9) CNTs at 280 K. Broken arrows are guide for eyes. Right: Arrangement of the dipole moment component along the CNT axis. The axial dipole moment of each water molecule is represented by red (blue) arrows when its value is zero or greater (less than zero).

ordered phase is rarely produced in pure ice because the disorder is practically frozen in before reaching the ordered phase due to the very slow kinetics of the proton reorientations at very low temperatures. Though the ordering transition can be catalyzed by doping with hydroxides, the ordered phase known as ice XI (Matsuo et al., 1986) has only been partially obtained (Tajima et al., 1982, 1984; Kawada, 1972, 1989). Researchers in this area are beginning to direct their attention to the outer solar system such as Pluto, where most water ice is considered to have existed in a crystalline phase for billions of years (Fukazawa et al., 2006). In marked contrast, we have shown that the proton-ordered water, FMW, can be produced at ambient conditions by utilizing the interior space of CNTs immersed in a reservoir water.

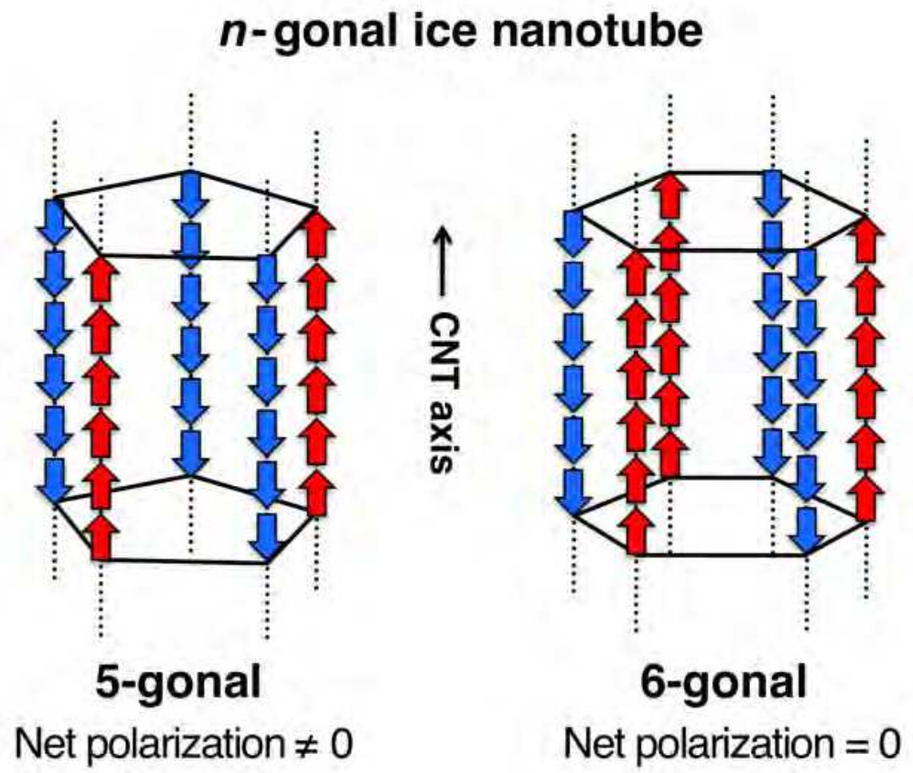

Fig. 8. Illustration of arrangement of the dipole moment component along the CNT axis for the 5- and 6-gonal ice nanotubes. Each dipole moment is represented by red (blue) arrows when its value is zero or greater (less than zero). Solid and broken lines are guide for eyes.

It is also worth referring to so far reported *n*-gonal ice-nanotubes. Those *n*-gonal ice-nanotubes have been found inside infinite or capped CNTs under high pressure/low temperature conditions with non-zero net spontaneous polarization (Luo et al., 2008; Mikami at al., 2009). Figure 8 shows schematic illustrations of the arrangement of the axial dipole moment for the 5- and 6-gonal ice nanotubes. Though each of the *n* wires of water molecules along the CNT axis is ferroelectric, the inter-wire relation is antiferroelectric. They are, therefore, not single-domain ferroelectric ice. In addition, non-zero net polarization arises only for an odd number of *n*. It should be noted that unlike the ice nanotubes, the FMW yields non-zero net polarization not only for the 5-gonal but also for the 6-gonal.

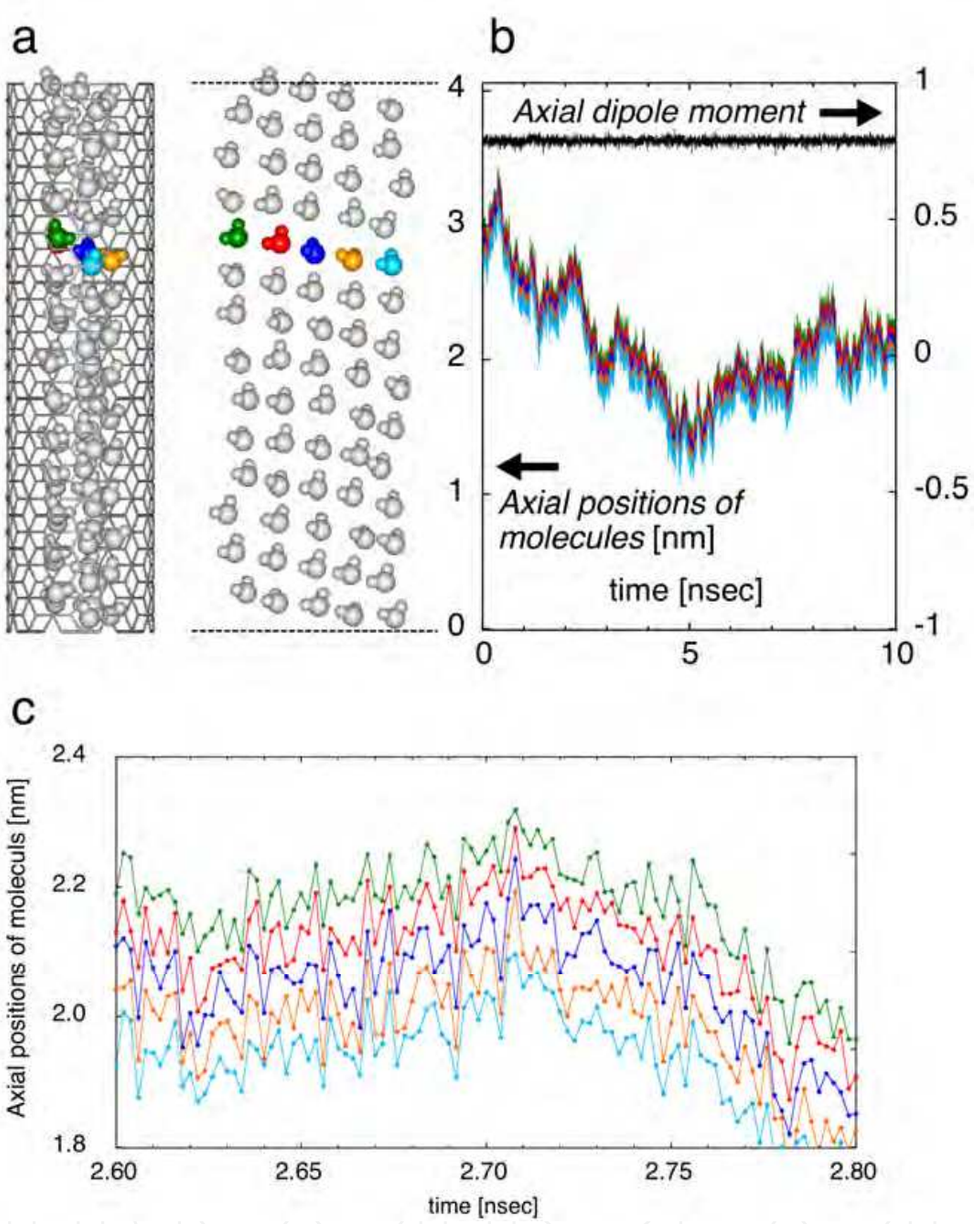

Fig. 9. Proton-ordered diffusion inside the (8, 8) CNT of length 4.0 nm. 280 K. (a) Unfolded-view snapshot. (b) Axial positions of five neighbouring molecules traced in corresponding colours. The net axial polarization of water inside the CNT traced in black (units are the magnitude of a single dipole of TIP5P-E water). a and b from Fig.2 of Nakamura & Ohno, 2011. Reproduced by permission of the PCCP Owner Societies. (c) A close-up of the motions between 2.6-2.8 nsec.

In general, a highly ordered structure such as the FMW seems suggestive of a rigid, immobile phase. Counter to our intuition, however, the FMW is dynamic. Figure 9a shows a side-view (left) and its corresponding unfolded-view snapshot obtained from the simulation employing the (8, 8) CNT. Five neighbouring molecules along the helix are coloured, and

their axial positions are traced in corresponding colours (Fig. 9b, c). The net axial polarization of the water inside the CNT is also shown in Fig. 9b (black line). The molecules diffuse along the CNT axis, keeping the proton-ordered network intact. They fluctuate and gradually shift away from their initial positions like a one-dimensional Brownian motion. A nanometre-order shift over nanosecond-order time is often seen. This concerted diffusion is termed 'proton-ordered diffusion.'

Figure 10 shows a series of elementary processes of the proton-ordered diffusion. Due to the single helical chain structure of the FMW, there are 'vacant pockets' in the interior space of the CNT near its both ends. The vacant pocket near the CNT top is filled molecule by molecule with reservoir water molecules. The molecules filling the pockets enter deeper and become more stable. At the same time, another vacant pocket is created at the same place again, which makes the filling process endless. A similar filling process also takes place near the bottom of the CNT. The proton-ordered diffusion is thus deeply relevant to the structure of the FMW.

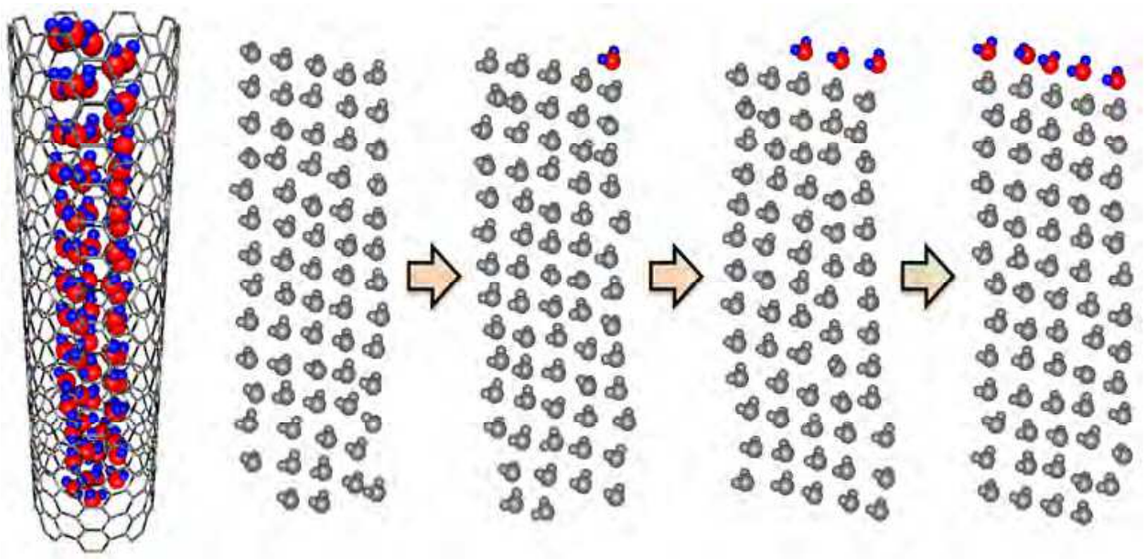

Fig. 10. Mechanism of the proton-ordered diffusion inside the (8, 8) CNT of length 4.0 nm. 280K. The oxygen (hydrogen) atoms of the water molecules entering from outside the CNT are colored red (blue).

The direction of the axial diffusion is practically dictated by the stochastic process near the CNT ends, and the probability of shifting in either directions is, on average, equal. From this viewpoint, a significant shift only in one direction seen in Fig. 9b might sound paradoxical. It is, however, understood by analogy with 'leads in a prolonged fair coin-tossing game.' When the cumulative number of heads is larger than that of tails, heads is in the lead (and vice versa). The leads are equivalent to the position shifts in the proton-ordered diffusion. When a great many series of fair coin-tossing games are conducted independently, the most likely result is for one side to be in the lead during the entire course of the game. This tendency becomes more pronounced for the games with a larger number of tosses. Contrary to popular notions, the least likely result is for the two sides to be tied for the time in the lead (Feller, 1968). The diffusion trajectory shown in Fig. 9b therefore represents a quite likely result.

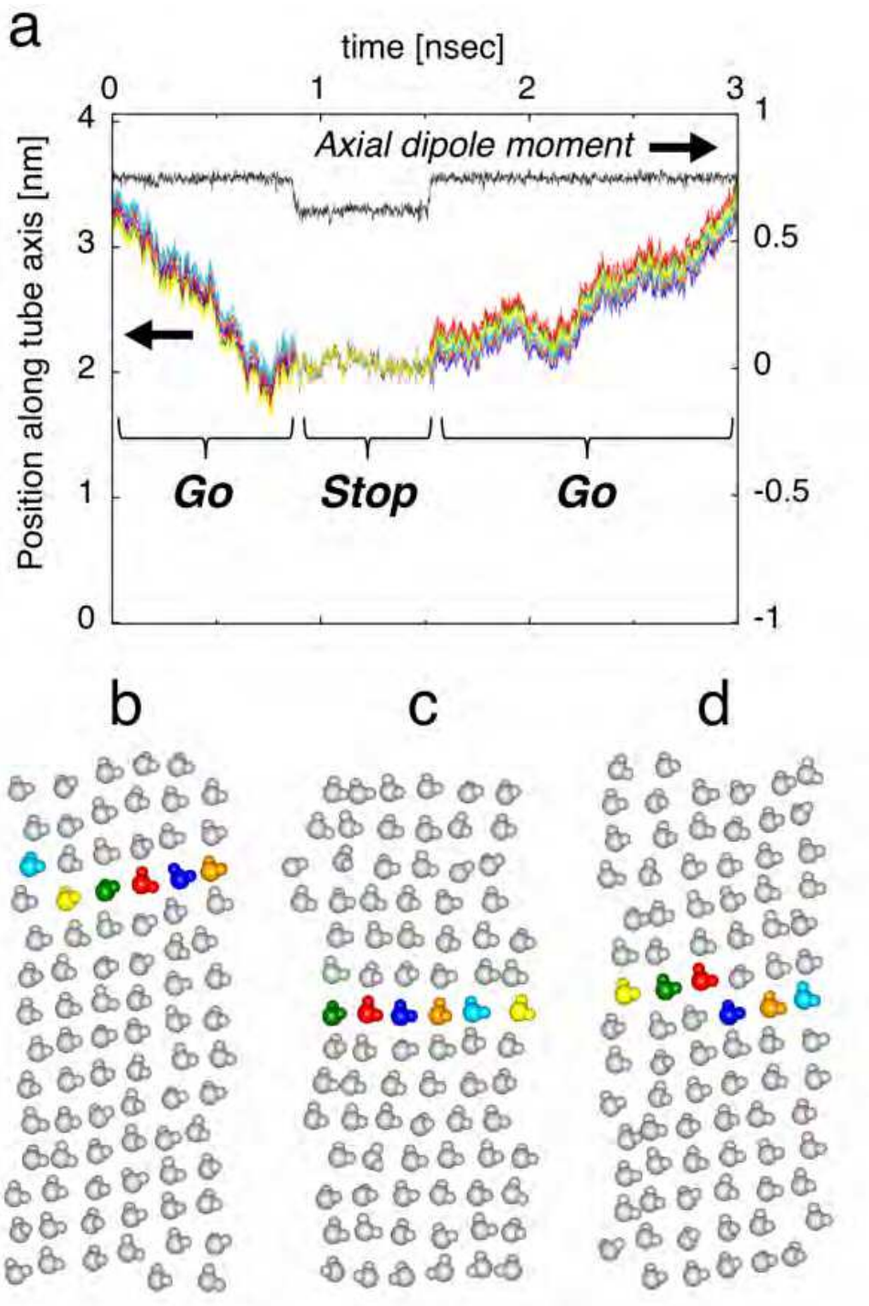

Fig. 11. 'Go–stop–go' motion of water inside the (9, 9) CNT of length 4.0 nm. 290 K. (a) Axial positions of six coloured molecules in the unfolded-view snapshots b, c, and d are traced in corresponding colours. The net axial polarization of water inside the CNT is traced in black (units are the magnitude of a single dipole of TIP5P-E water). Unfolded-view snapshot at (b) 0.072 ns, (c) 1.214 ns, and (d) 1.998 ns. From Fig.3 of Nakamura & Ohno, 2011. Reproduced by permission of the PCCP Owner Societies.

The proton-ordered diffusion is also observed for the FMW inside the (9, 9) CNTs (Fig. 11). Looking into the axial positions of six marked molecules, we notice that they are

temporarily pinned at a certain axial position (at about 2.0 nm, from 0.9 to 1.5 ns in Fig. 11a). Before the pinning takes place, the confined water has a single-helix structure (b) and undergoes the axial diffusion. When pinned, however, it is no longer helical: it transforms into axially stacked layers of water molecules and consequently all the molecules become practically immobile (c). Once the pinning ends, the water recovers the FMW structure and resumes the proton-ordered diffusion (d). These motion changes literally correspond to 'Go-Stop-Go.'

In Fig. 11a, the net axial polarization of the confined water is also plotted. It should be noted that the 'Go-Stop-Go' is accompanied by step-wise changes of the net polarization. As we see the series of unfolded snapshots (b, c, d), each dipole axis comes to slightly tilt against the CNT axis when the pinning takes place, which results in a lower net polarization than that of the FMW during the pinning.

We have performed a long-time simulation with a shorter (9, 9) CNT of length 2.1 nm, in which we find a series of stepwise changes of the net polarization (Fig. 12a). Amazingly, the values fall on any one of the nine lines. Five independent phases, labeled '0' to '4', are suggested. Phase #4 corresponds to the FMW, the most stable phase (Nakamura & Ohno, 2011). Figure 12b shows unfolded-view snapshots from each phase, which is helpful to understand how the net polarization is digitized. The molecules are coloured red (blue) when their axial dipole moment P_z is zero or greater (less than zero). Each axial water wire is red or blue, i.e., ferroelectric. The ice rule is practically obeyed for all the snapshots. Under the ice rule, many other dipole arrangements are possible for each phase except #4.

Phase #0 is very similar to the reported 6-gonal ice nanotubes (Luo et al., 2008; Mikami at al., 2009) in that the inter-wire relation is antiferroelectric though the intra-wire is ferroelectric, resulting in a zero net spontaneous polarization. In phase #1 (#2), the axial water wires in red outnumber those in blue by two (four). The redundant water wires yield a non-zero net polarization. Phases #3 and #4 have no domain boundary along the CNT axis.

We detail the transition from one phase to the other, e.g., from phase #0 to #1 (at around 18 ns, indicated by a yellow arrow in Fig. 12a). A sequence of the transient snapshots is shown in Fig. 12c. At $\Delta t = 0$, the inter-wire relation is antiferroelectric. Under local perturbation from the reservoir water, the dipole orientation of the encircled molecule is changed so as to introduce a domain boundary in the axial water wire ($\Delta t = 3.5$ ps), which corresponds to a hydrogen bonding defect (Dellago et al., 2003; Köfinger et al., 2008; Köfinger & Dellago, 2009). The ice rule is consequently breached at the domain boundary, and local instability is created. Fluctuating rapidly along the CNT axis, the position of the domain boundary shifts toward the opposite CNT edge accompanied by the dipole reorientations ($\Delta t = 4.7$ ps). Eventually the whole water wire becomes red ($\Delta t = 8.5$ ps). Triggered by the local perturbation, the phase transition is thus completed in less than 10 ps. It should be noted that the perturbation from the reservoir water only works on the dipole reorientation and has little effect on their diffusion. This is the case for phases #0 to #3. In marked contrast, for phase #4, the local perturbation has little effect on the dipole reorientation: it only works on the diffusion of the molecules, that is, the proton-ordered diffusion of the FMW.

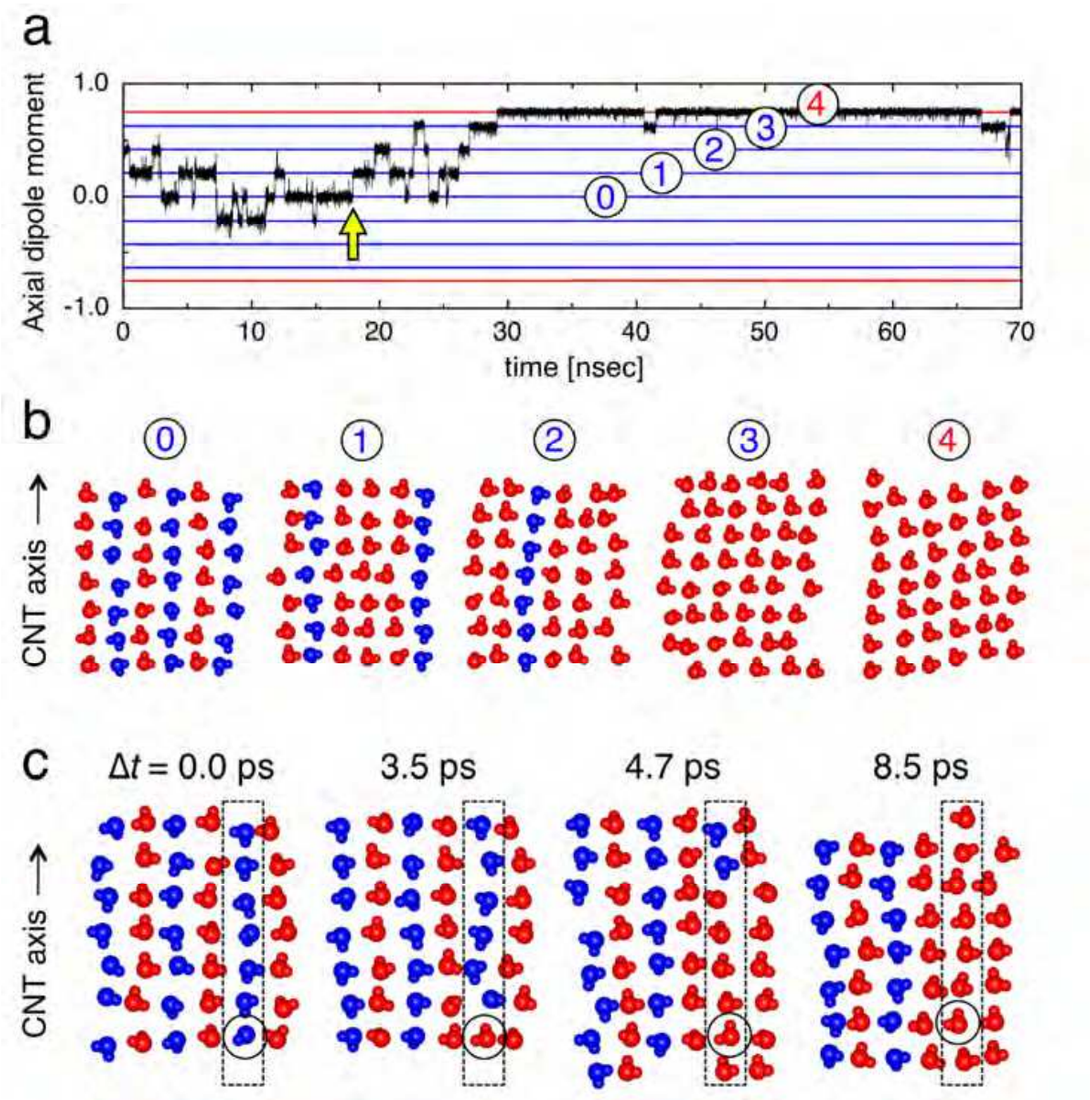

Fig. 12. Sequence of spontaneous transitions with step-wise changes of net polarization of water inside the (9, 9) CNT of length 2.1 nm. 280 K. (a) Net axial polarization of water traced in black (units are the magnitude of a single dipole of TIP5P-E water). Two red lines represent the ferroelectric mobile water. Seven blue lines the immobile water. Labels '0' to '4' on five lines represent five independent water phases. (b) Unfolded-view snapshots from each phase. Water molecules are colored red (blue) when their axial dipole moment P_z is zero or greater (less than zero). (c) Sequence of unfolded-view snapshots during the transition from phase #0 to #1, which is indicated by yellow arrow in (a). Black circles and dotted rectangles are guide for eyes. From Fig.4 of Nakamura & Ohno, 2011. Reproduced by permission of the PCCP Owner Societies.

Here, a question still remains: how the mobile phase, the FMW, is reached from the immobile phases? This process is clearly explained in Fig. 13. A schematic, representative arrangement of the confined water molecules for phase #0 to #2, all of which have axial domain boundaries, are shown in (a). In these phases, the fluctuation in directions

perpendicular to the CNT axis ('lateral fluctuation') is severely restricted due to the proton-proton repulsion as shown in the yellow areas in (b). For phase #3, which has no axial domain boundary, there are two representative arrangements: domain-boundary-free (c) and lateral domain boundaries included (f).

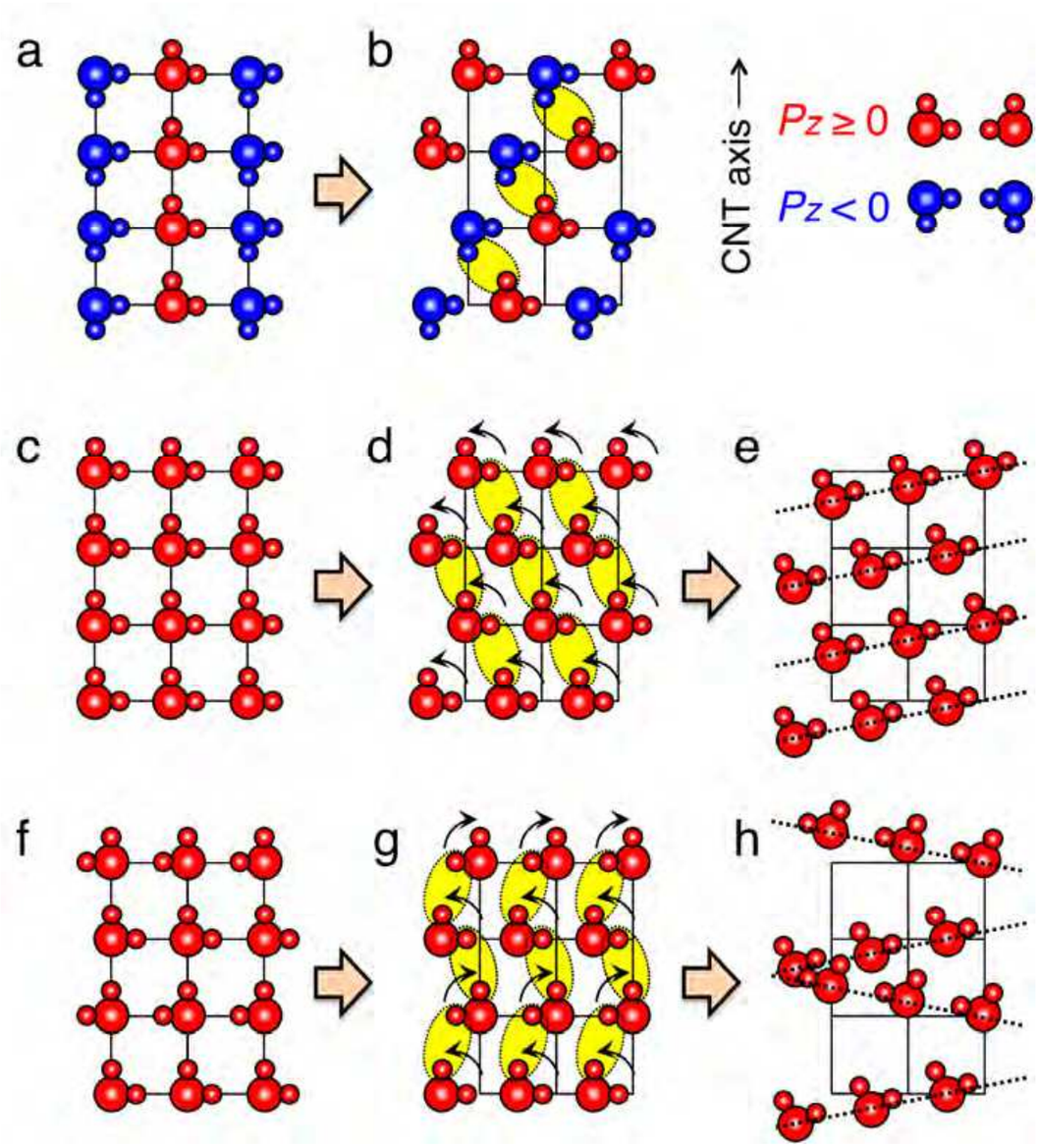

Fig. 13. Proton ordering and thermal fluctuation explained with schematic unfolded views (for simplicity, square lattice is used). Left: Without fluctuation. (a) Axial (vertical) domain boundaries included. (c) Domain-boundary-free. (f) Lateral domain boundaries included. Middle: With lateral fluctuation. (b), (d) and (g) correspond to distorted structure examples of (a), (c), and (f), respectively, under lateral fluctuation. Yellow represents repulsions induced by the lateral fluctuation. Arrows in (d) and (g) represent the rotational direction of each dipole. Right: Resultant arrangements. (e) Ferroelectric mobile water reached via (d). (h) Example of unstable arrangements reached via (g). Black dotted lines are guide for eyes.

In the domain-boundary-free case (c), the repulsion also arises under the lateral fluctuation (d). It can, however, be avoided by slightly tilting each dipole orientation toward the CNT axis (indicated by arrows) and giving the axial positions a slight downward slope along the lateral direction (e). The molecules thus align along the single helix running through the CNT without breaching the ice rule. This also gives the reason why phase #4 yeilds spontaneous polarization larger than that of phase #3. In the other case (f), however, avoiding the proton-proton repulsion induced by the lateral fluctuation only leads to instability elsewhere (g to h). More dominant the domain-boundary-free arrangement (c), the more likely the transition from phase #3 to #4 takes place.

5. Effect of different models

Based on the TIP5P-E water model, we have seen the quite unusual behaviour of water molecules inside the (8, 8) and the (9, 9) CNTs, i.e., that formation of single-domain ferroelectric water (FMW) and its concerted diffusion (proton-ordered diffusion). We have also seen in Fig. 5 that for these 'critical' CNT diameters (about 1.1-1.2 nm) there are non-trivial differences in water density among the water models, which strongly suggests that the confined water structure needs to be examined model by model under the same conditions as used for the TIP5P-E water simulations above.

Figure 14 shows the top-view snapshots and net axial polarization of water inside the (9, 9) CNT obtained for each water model, together with unfolded-view snapshot examples for the SPC/E model. The top-view snapshots for the TIP3P and the TIP4P reveal thicker water tubes compared to the SPC/E (and TIP5P-E, see Fig. 5c), clearly demonstrating model dependence. The time evolution of the net axial polarization P_z for the TIP3P and the TIP4P reveals considerable fluctuation (Fig. 14a and b, right-hand side). In contrast, a series of stepwise changes is seen for the SPC/E (Fig. 14c, right-hand side). The values fall on any of three lines, suggesting two independent phases.

We see the relation between the two phases of the SPC/E water and their corresponding molecular structure. As well as phase #0 introduced in the TIP5P-E simulations (labeled '0' in Fig. 12b), the antiferroelectric relation between the SPC/E water wires along the CNT axis yields the phase with $P_z = 0$, which is therefore named phase #0 based on the same naming scheme as used in the TIP5P-E water simulations. The transitions to the other magnitude of P_z (i.e, phase #1) take place by the flip of the water wire direction, similarly to those demonstrated in the TIP5P-E simulations (Fig. 12c). Phase #0 and #1 consist of axially stacked layers of anomalously immobile water molecules, which are essentially the same for the corresponding phases of the confined TIP5P-E water. It should be note that for the TIP5P-E, there are five independent phases (#0 to #4). For the SPC/E, however, only phase #0 and #1 are observed and the other phases including the FMW (i.e., phase #4) are not observed. The effect of the choice of model between the SPC/E and the TIP5P-E is thus clear.

Also for the (8, 8) CNT, the model dependence is significant (Fig. 15). The top-view snapshot for the TIP3P reveals a thick, less ordered tube structure (a), whereas the TIP4P and the SPC/E reveal a 4-gonal water tube (b and c). The net axial polarization P_z for the TIP3P water shows a considerable fluctuation (a, right-hand side). For the TIP4P and the SPC/E, the fluctuation is fairly suppressed and most of the values of P_z fall on any of five lines, suggesting three independent phases (b and c, right-hand side).

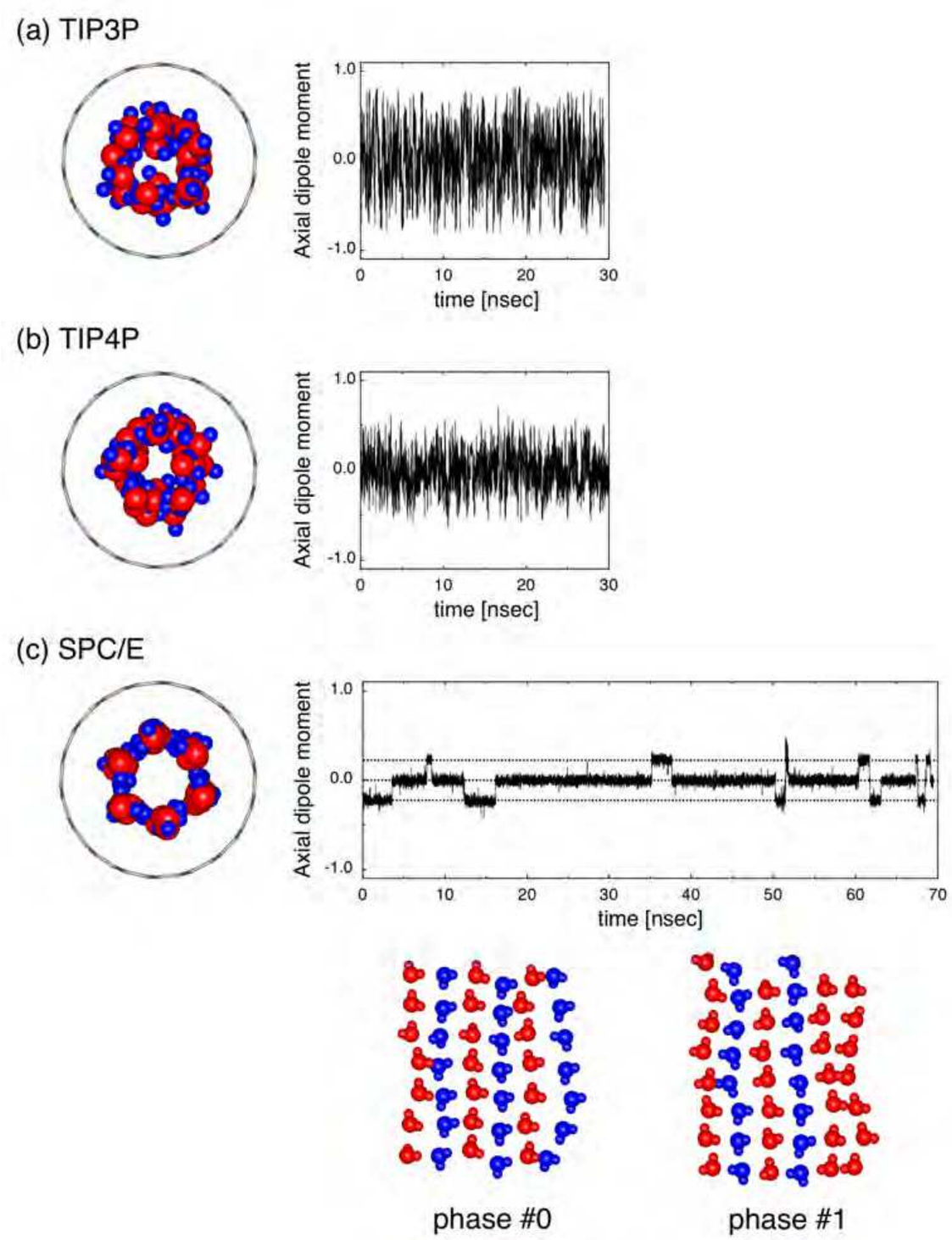

Fig. 14. Top-view snapshots and net axial polarization of water inside the (9, 9) CNT of 2.1 nm length for each water model. 280K. For SPC/E model, unfolded-view snapshot examples for phase #0 and #1 are also shown. Polarization and unfolded-view results are adapted from Fig.3 of Nakamura & Ohno, 2012a.

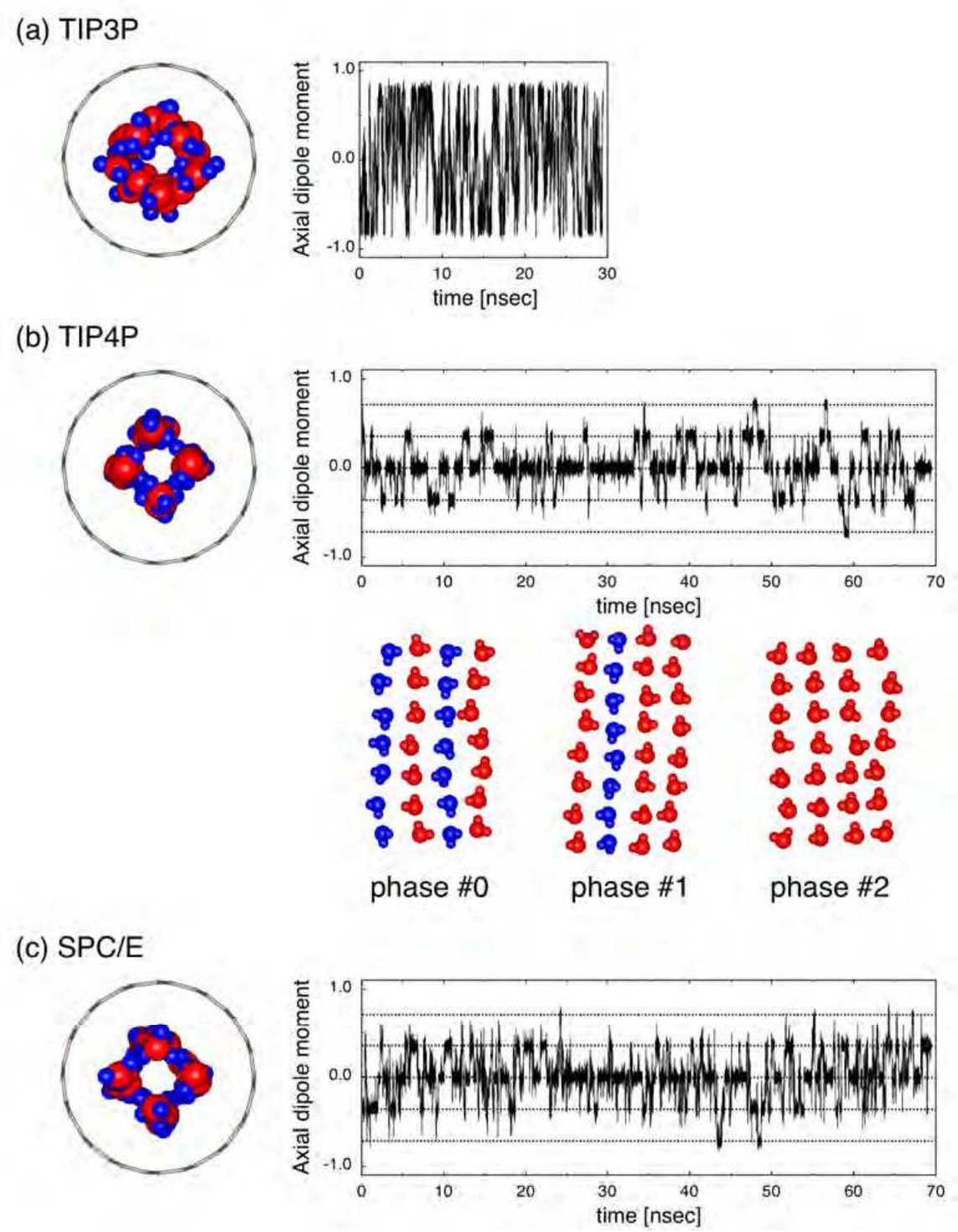

Fig. 15. Top-view snapshots and net axial polarization of water inside the (8, 8) CNT of 2.1 nm length for each water model. 280K. For TIP4P model, unfolded-view snapshot examples for phase #0 to #2 are also shown. Polarization and unfolded-view results are adapted from Fig.5 of Nakamura & Ohno, 2012a.

Examples of unfold-view snapshots corresponding to the three independent phases (phase #0 to #2) for the TIP4P are shown on the right-hand side of Fig. 15b. The transition mechanism between the phases is essentially the same as that described earlier. Unlike the confined TIP5P-E revealing the 5-gonal water tube (Fig. 5b), the TIP4P and the SPC/E reveal the 4-gonal tubes (Fig. 15b and c, left-hand side). In addition, the transition to the phase #4 (the FMW) is not observed for both the TIP4P and the SPC/E. The single helix structure of the TIP5P-E water very efficiently fills the interior space of the (8, 8) CNTs compared to the water structures of the other water models, resulting in the highest water density. We note that for the TIP5P-E water, the shorter the (8, 8) CNT length, the more often a 4-gonal single helix water structure is observed. The 4-gonal FMW is, however, rarely observed for the (8, 8) CNTs of length about 2-4 nm compared to the 5-gonal single helix water structure.

We have seen that both for the (8, 8) and the (9, 9) CNTs, the TIP3P water results in a less ordered structure compared to the other water models. The main reason for this is possibly attributed to too fast dynamics of the TIP3P water, which gives the self-diffusion constant of bulk liquid water more than double the experimental one. The reported values (25 ˚C, in the unit of 10^{-5} cm^2/sec) are 2.3 for experiment, 5.19 for TIP3P, 2.49 for SPC/E, 3.29 for TIP4P, and 2.80 for TIP5P-E (Mahoney & Jorgensen, 2001; Mark & Nilsson, 2001; Mills, 1973; Price et al., 1999). The structural ordering of the confined TIP3P water molecules is considered to be interrupted by the unrealistic fluctuation. Here, we briefly refer to a report on H_2O/CNT simulations employing a 'modified TIP3P' model. Though this model's diffusion constant is as high as the original TIP3P, a twisted-column shape of water inside the (7, 7), (8, 8) and (9, 9) CNTs was reported at ordinary ambient conditions (Noon et al., 2002). In the modified TIP3P model, the Lennard-Jones parameters on the hydrogen atoms were newly introduced to avoid singularities in integral equation calculations of activation free energies in complex molecular systems (Neria, 1996). The additional parameters, however, do not correct the original TIP3P's well-documented shortcomings including the very high diffusion constant (Mark & Nilsson, 2001). The effect of the additional parameters is therefore considered to be so strong that the ordered structures become possible despite the high diffusion constant.

For the rest of the water models (SPC/E, TIP4P, TIP5P-E), the model dependence has also been observed. The SPC/E and the TIP4P water molecules form into the axially stacked layers of anomalously immobile water molecules. The resultant water phases, however, correspond to the metastable phases of the confined TIP5P-E water, whose stable phase, the FMW, has not been observed for the SPC/E and the TIP4P models. What makes this difference? We pay attention to the fact that among those water models, the TIP5P-E most realistically describes the molecular charge distribution by explicitly taking into account the negative charges along the lone-pair directions of the water molecule. In the TIP4P model, the negative charge is placed on an additional fictive site other than the oxygen atom site. The number of electrostatic interaction sites, however, is three as well as the TIP3P model. Accuracy in the description of the molecular charge distribution is considered to be crucial in simulating the water inside the CNTs of the 'critical' diameters.

6. Conclusion

We have reported recent progress of H_2O/CNT simulations, focusing on the unusual behavior of the confined water molecules and the effect of the water models with different

numbers of interaction sites (from three to five sites). All the models commonly show that the unusual behavior of the confined water changes in accordance with the CNT diameter size. We have found a critical CNT diameter range (about 1.1-1.2 nm), for which significant anomalous behavior of water that differs from model to model is observed. Except for this range, significant differences between the models have not been found. Based on the 5-site water models, which most realistically describes the molecular charge distribution among the water models used, single-domain ferroelectric water is produced at ambient conditions. The ferroelectric water diffuses while keeping its proton-ordered network intact. The mobile/immobile water transitions accompanied by the step-wise changes in net polarization of water have also been found. The outcome is expected to enable examining the ferroelectricity by detecting an abrupt change in mobility of water molecules, as well as calorimetry and dielectric experiments. Simulations based on the first-principles are also highly desirable to confirm the ferroelectric water. Such studies are now under way.

7. References

Alexiadis, A. & Kassinos, S. (2008a). The density ofwater in carbon nanotubes. *Chemical Engineering Science,* 63, pp. 2047 – 2056.

Alexiadis, A. & Kassinos, S. (2008b). Molecular Simulation of Water in Carbon Nanotubes. *Chemical Reviews,* 108, pp. 5014–5034.

Bai, J.; Wang, J. & Zeng, X. C. (2006). Multiwalled ice helixes and ice nanotubes. *Proceedings of the National Academy of Sciences,* 103, pp. 19664-19667.

Bernal, J. D. & Fowler, R. H. (1933). A Theory of Water and Ionic Solution, with Particular Reference to Hydrogen and Hydroxyl Ions. *Journal of Chemical Physics,* 1, pp.515-548.

Berendsen, H. J. C.; Grigera, J. R. & Straatsma, T. P. (1987). The missing term in effective pair potentials. *Journal of Physical Chemistry,* 91, pp. 6269-6271.

Berendsen, H. J. C.; Postma, J. P. M.; van Gunsteren, W. F. & Hermans, J. (1981). Interaction models for water in relation to protein hydration, In: *Intermolecular Forces,* B. Pullman, (Ed.), pp. 331-342, Reidel, Dordrecht

Bramwell, S. T. (1999). Ferroelectric ice. *Nature,* 397, pp. 212-213.

Case, D. A; Darden, T. A.; Cheatham, T. E. III; Simmerling, C. L.; Wang, J.; Duke, R. E.; Luo, R.; Merz, K. M.; Pearlman, D. A.; Crowley, M.; Walker, R. C.; Zhang, W.; Wang, B.; Hayik, S.; Roitberg, A.; Seabra, G.; Wong, K. F.; Paesani, F.; Wu, X.; Brozell, S.; Tsui, V.; Gohlke, H.; Yang, L.; Tan, C.; Mongan, J.; Hornak, V.; Cui, G.; Beroza, P.; Mathews, D. H.; Schafmeister, C.; Ross, W. S. & Kollman, P. A. (2006). *AMBER 9*. University of California, San Francisco.

Darden, T.; York, D. & Pedersen, L. (1993). Particle mesh Ewald: An *N*-log (*N*) method for Ewald sums in large systems. *Journal of Chemical Physics,*98, pp. 10089-10092.

Dellago, C.; Naor, MM. & Hummer, G. (2003). Proton Transport through Water-Filled Carbon Nanotubes. *Physical Review Letters,* 90, 105902.

Feller, W. (1968). Fluctuations in Coin Tossing and Random Walks. In: *An Introduction to Probability Theory and Its Applications,* ch. 3, Wiley, USA

Fernández, R. G.; Abascal, J. L. F. & Vega, C. (2006). The melting point of ice Ih for common water models calculated from direct coexistence of the solid-liquid interface. *Journal of Chemical Physics,* 124, 144506.

Fukazawa, H.; Hoshikawa, A.; Ishii, Y.; Chakoumakos, B. C. & Fernandez-Baca, J. A. (2006). Existence of ferroelectric ice in the universe. *The Astrophysical Journal,* 652, L57–L60.

Hummer, G.; Rasaiah, J. C. & Noworyta, J. P. (2001). Water conduction through the hydrophobic channel of a carbon nanotube. *Nature,* 414, pp. 188-109.

Iedema, M. J.; Dresser, M. J.; Doering, D. L.; Rowland, J. B.; Hess, W. P.; Tsekouras, A. A. & Cowin, J. P. (1998). Ferroelectricity in Water Ice. *Journal of Physical Chemistry B,* 102, pp. 9203-9214.

Jackson, S. M. & Whitworth, R. W. (1995). Evidence for ferroelectric ordering of ice Ih. *Journal of Chemical Physics,* 103, pp.7647-7648.

Jackson, S. M.; Nield, V. M.; Whitworth, R. W.; Oguro, M.; Wilson, C. C. (1997). Single-Crystal Neutron Diffraction Studies of the Structure of Ice XI. *Journal of Physical Chemistry B,* 101, pp. 6142-6145.

Jorgensen, W. L.; Chandrasekhar, J.; Madura, J. D.; Impey, R. W. & Klein, M. L. (1983). Comparison of simple potential functions for simulating liquid water. *Journal of Chemical Physics,* 79, pp. 926-935.

Kawada, S. (1972). Dielectric Dispersion and Phase Transition of KOH Doped Ice. *Journal of the Physical Society of Japan,* 32, pp. 1442-1442.

Kawada, S. (1989). Acceleration of dielectric relaxation by koh-doping and phase transition in ice Ih. *Journal of Physics and Chemistry of Solids,* 50, pp. 1177-1184.

Koga, K.; Gao, G. T.; Tanaka, H. & Zeng, X. C. (2001). Formation of ordered ice nanotubes inside carbon nanotubes. *Nature,* 412, pp. 802-805.

Köfinger, J.; Hummer, G. & Dellago, C. (2008). Macroscopically ordered water in nanopores. *Proceedings of the National Academy of Sciences,* 105, pp.13218–13222.

Köfinger, J. & Dellago, C. (2009). Orientational Dynamics and Dielectric Response of Nanopore Water. *Physical Review Letters,* 103, 080601.

Luo, C. F.; Fa, W.; Zhou, J.; Dong, J. M. & Zeng, X. C. (2008). Ferroelectric Ordering in Ice Nanotubes Confined in Carbon Nanotubes. *NANO LETTERS,* 8, pp. 2607-2612.

Liu, Y.; Wang, Q.; Wu, T. & Zhang, L. (2005). Fluid structure and transport properties of water inside carbon nanotubes. *Journal of Chemical Physics,* 123, 234701.

Mahoney, M. W. & Jorgensen, W. L. (2000). A five-site model for liquid water and the reproduction of the density anomaly by rigid, nonpolarizable potential functions. *Journal of Chemical Physics,* 112, pp. 8910-8922.

Mahoney, M. W. & Jorgensen, W. L. (2001). Diffusion constant of the TIP5P model of liquid water. *Journal of Chemical Physics,* 114, pp. 363-366.

Mark, P. & Nilsson, L. (2001). Structure and Dynamics of the TIP3P, SPC, and SPC/E Water Models at 298 K. *Journal of Physical Chemistry A,* 105, pp. 9954-9960.

Mashl, R. J.; Joseph, S.; Aluru, N. R. & Jakobsson, E. (2003). Anomalously Immobilized Water: A New Water Phase Induced by Confinement in Nanotubes. *NANO LETTERS,* 3, pp. 589-592.

Matsuo, T.; Tajima, Y. & Suga, H. (1986). CALORIMETRIC STUDY OF A PHASE TRANSITION IN D_2O ICE Ih DOPED WITH KOD: ICE XI. *Journal of Physics and Chemistry of Solids,* 47, pp. 165-173.

Mikami, F.; Matsuda, K.; Kataura, H. & Maniwa, Y. (2009). Dielectric Properties of Water inside Single-Walled Carbon Nanotubes. *ACS NANO,* 3, pp. 1279–1287.

Mills, R. (1973). Self-Diffusion in Normal and Heavy Water in the Range 1-45. *Journal of Physical Chemistry,* 77, pp. 685-688.

Nakamura, Y. & Ohno, T. (2011). Ferroelectric mobile water. *Physical Chemistry Chemical Physics,* 13, pp. 1064–1069.

Nakamura, Y. & Ohno, T. (2012a). Structure of water confined inside carbon nanotubes and water models. *Materials Chemistry and Physics, 132, pp. 682–687.*

Nakamura, Y. & Ohno, T. (2012b). Single-Domain Ferroelectric Water and its Concerted Diffusion in Nanotubes. Materials Science Forum, 700, pp. 108-111.

Neria, E. (1996). Simulation of activation free energies in molecular systems. *Journal of Chemical Physics,* 105, pp. 1902–1921.

Noon, W. H.; Ausman, K. D.; Smalley, R. E. & Ma, J. (2002). Helical ice-sheets inside carbon nanotubes in the physiological condition. *Chemical Physics Letters,* 355, pp. 445–448.

Pauling, L. (1935). The Structure and Entropy of Ice and of Other Crystals with Some Randomness of Atomic Arrangement. *Journal of the American Ceramic Society,* 57, pp. 2680-2684.

Price, W. L.; Ide, H. & Arata, Y. (1999). Self-Diffusion of Supercooled Water to 238 K Using PGSE NMR Diffusion Measurements. *Journal of Physical Chemistry A,* 103, pp. 448-450.

Rick, S. W. (2004). A reoptimization of the five-site water potential TIP5P for use with Ewald sums. *Journal of Chemical Physics,* 120, pp. 6085-6093.

Slater, J. C. (1941). Theory of the Transition in KH_2PO_4. *Journal of Chemical Physics,* 9, pp.16-33.

Su, X.; Lianos, L.; Shen, Y. R. & Somorjai, G. A. (1998). Surface-Induced Ferroelectric Ice on Pt(111). *Physical Review Letters,* 80, pp.1533-1536.

Tajima, Y.; Matsuo, T. & Suga, H. (1982). Phase transition in KOH-doped hexagonal ice. *Nature,* 299, pp. 810-812.

Tajima, Y.; Matsuo, T. & Suga, H. (1984). Calorimetric study of phase transition in hexagonal ice doped with alkali hydroxides. *Journal of Physics and Chemistry of Solids,* 45, pp. 1135-1145.

Vega, C.; Sanz, E. & Abascal, J. L. F. (2005). The melting temperature of the most common models of water. *Journal of Chemical Physics,* 122, 114507.

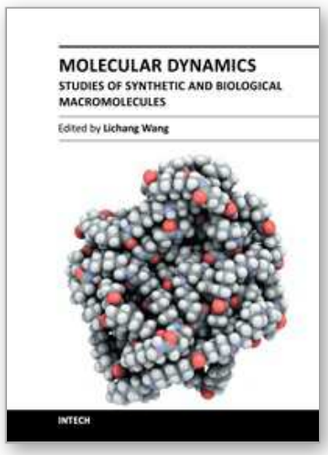

Molecular Dynamics - Studies of Synthetic and Biological Macromolecules

Edited by Prof. Lichang Wang

ISBN 978-953-51-0444-5
Hard cover, 432 pages
Publisher InTech
Published online 11, April, 2012
Published in print edition April, 2012

Molecular Dynamics is a two-volume compendium of the ever-growing applications of molecular dynamics simulations to solve a wider range of scientific and engineering challenges. The contents illustrate the rapid progress on molecular dynamics simulations in many fields of science and technology, such as nanotechnology, energy research, and biology, due to the advances of new dynamics theories and the extraordinary power of today's computers. This second book begins with an introduction of molecular dynamics simulations to macromolecules and then illustrates the computer experiments using molecular dynamics simulations in the studies of synthetic and biological macromolecules, plasmas, and nanomachines. Coverage of this book includes: Complex formation and dynamics of polymers Dynamics of lipid bilayers, peptides, DNA, RNA, and proteins Complex liquids and plasmas Dynamics of molecules on surfaces Nanofluidics and nanomachines

InTech Europe
University Campus STeP Ri
Slavka Krautzeka 83/A
51000 Rijeka, Croatia
Phone: +385 (51) 770 447
Fax: +385 (51) 686 166
www.intechopen.com

InTech China
Unit 405, Office Block, Hotel Equatorial Shanghai
No.65, Yan An Road (West), Shanghai, 200040, China
中国上海市延安西路65号上海国际贵都大饭店办公楼405单元
Phone: +86-21-62489820
Fax: +86-21-62489821

IntechOpen